

Exploring the Interaction of BeS Monolayer and Lung Disease Biomarkers: Potential Material for Biosensing Applications

Sudipta Saha and Md. Kawsar Alam¹

Department of Electrical and Electronic Engineering, Bangladesh University of Engineering and Technology,
Dhaka- 1205, Bangladesh

Abstract

Considerable attention has been directed towards the prognosis of lung diseases primarily due to their high prevalence. Despite advancements in detection technologies, current methods such as computed tomography, chest radiographs, bold proteomic patterns, nuclear magnetic resonance, and positron emission tomography still face limitations in detecting diseases related to the lungs. Consequently, there is a need for swift, non-invasive and economically feasible detection methods. Our study explores the interaction between BeS monolayer and breathe biomarkers related to lung disease utilizing the density functional theory (DFT) method. Through comprehensive DFT analysis, including electronic properties analysis, charge transfer evaluations, work function, optical properties assessment and recovery times, the feasibility and efficiency of BeS as a VOC (volatile organic compound) detection are investigated. Findings reveal significant changes in bandgap upon VOC adsorption, with notable alteration in work function for selective compounds. Optical property analyses demonstrate the potential for selective detection of biomarkers within specific wavelength ranges. Moreover, the study evaluates the impact of electric fields and strain on VOC-2D BeS interaction. Furthermore, the desorption of these VOCs from the BeS surface can be achieved through a heating process or under the illumination of UV light. This feature enables the reusability of the 2D material for biosensing applications. These findings highlight the potential of the BeS monolayer as a promising material for the sensitive and selective detection of breath biomarkers related to lung disease.

¹ Corresponding Author. Email: kawsaralam@eee.buet.ac.bd; kawsar.alam@alumni.ubc.ca

Introduction

Lung diseases encompass many conditions that affect the lungs, including infections, chronic respiratory diseases, and lung cancer. These diseases can significantly impact an individual's respiratory function and overall health. Common examples of lung diseases include asthma, chronic obstructive pulmonary disease (COPD), pneumonia, and lung cancer. Notably, lung cancer has consistently held the title of the most frequently diagnosed cancer worldwide for several decades [1]. In recent years, technologies like computed tomography (CT) [2,3], chest radiographs (CXR) [4], positron emission tomography (PET) [5], bold proteomic patterns [6], nuclear magnetic resonance (NMR) [7], magnetic resonance imaging (MRI) [5] and have gained extensive usage in clinical settings for the detection of various lung diseases. Despite their effectiveness, these methods come with significant drawbacks; for instance, conventional X-rays (CXR), CT scans, and PET scans entail radiation exposure risks [8,9], high operational costs [10,11] and limitations in providing a conclusive diagnosis only at advanced stages of the particular disease. Thus, these techniques still fall short in detecting the early stages of the disease and fail to enhance survival rates for patients notably [12]. Due to these limitations, a swift, non-invasive, and economically feasible means of detecting lung diseases holds significant value. Researchers are presently investigating novel methods to detect diseases in their early stages. Exhaled human breath emerges as a promising, cost-effective, and swift approach for detection [13,14]. Volatile organic compounds (VOCs), including hydrocarbons like isoprene (C_5H_8), hydrocarbon derivatives such as 2-propenal (C_3H_4O), 4-hydroxyhexanal ($C_6H_{10}O_2$) and acetone (C_3H_6O), along with diverse aromatic hydrocarbons like benzene (C_6H_6), act as biomarkers signifying the extent of lung diseases in humans (**Figure 1**) [15-18]. Recent progress in utilizing 2D materials for detecting biomarkers has received considerable attention [19-21]. The application of 2D materials, characterized by their high surface-to-volume ratio, shows promising prospects for enabling sensing at concentrations as low as a few ppb (parts per billion), thus achieving remarkable sensitivity [22,23]. In prior research, it was demonstrated that MoS_2 [24], $MoSe_2$ [25], SnS_2 [26] and WSe_2 [27] were proposed as biosensors for detecting lung cancer through exhaled breath analysis. Additionally, various forms of metal doping have been incorporated into MoS_2 , $MoSe_2$, and SnS_2 to enhance their sensing capabilities [24,26,28-30]. A first principle investigation into the functionalization of titanium carbide Ti_3C_2 MXenes was conducted to observe the detection of biomarkers related to lung cancer [31]. In VOC detection, group II-VI monolayers such as BeS, MgO and BeSe have received little attention recently. Theoretical predictions suggest that the BeS monolayer features a considerably wide bandgap and notable electronic and optical properties [32,33]. Furthermore, the BeS monolayer has demonstrated potential in gas sensing applications [34]. However, utilizing the BeS monolayer for identifying lung disease biomarkers is yet to be explored. The remarkable optical and electronic properties of the BeS monolayer, combined with its effectiveness in gas sensing and capture, have inspired the present study to investigate its prospect for sensing application of diseases related to lungs utilizing this 2D material. The interaction process has been thoroughly examined by assessing parameters including adsorption energy, bond or interaction distance, electron density difference and charge transfer. Furthermore, analysis of the PDOS (partial density of states) and electronic band structure has been done to study the electronic properties of the VOC adsorbed system. Exploring the feasibility of using this

material for biosensing application, various parameters such as conductivity, work function, reflectivity, absorbance and recovery time for all VOC adsorbed systems have been computed. Additionally, interaction has been observed under the influence of electric field and strain. The following sections provide detailed explanations of the computational methodology, procedures, and study results.

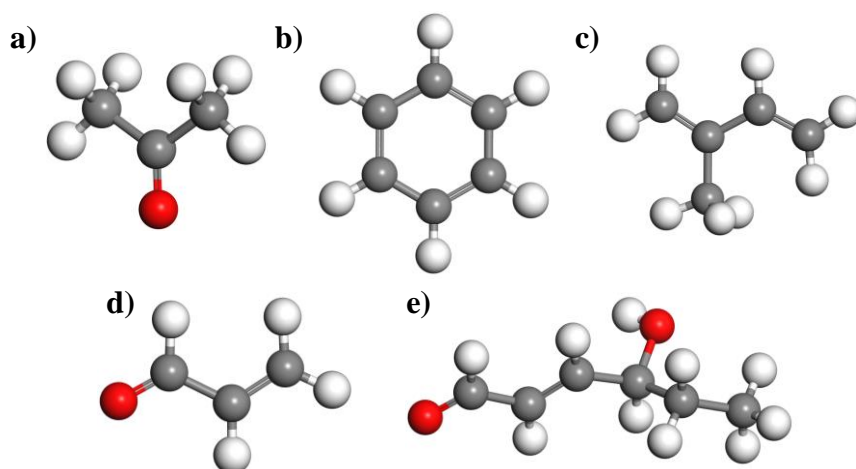


Figure 1. Volatile organic compounds linked to lung diseases (a) acetone, (b) benzene, (c) isoprene, (d) 2-propenal and (e) 4-hydroxy hexanal. Here, white, grey, and red spheres represent hydrogen, carbon, and oxygen atoms, respectively.

Computational Description and Methodology

In this study, density functional theory (DFT) calculations were performed utilizing the DMol³ [35] and CASTEP [36] modules of Materials Studio. Various computational analyses were conducted, including geometry optimization, electronic band structure analysis, density of states calculation, and Hirshfeld charge analysis using the DMol³ module. In contrast, phonon dispersion, electron density difference, and optical property assessment were performed using the CASTEP module. The study was conducted with a 3×3 supercell extracted from bulk BeS crystal, with a 21Å vacuum slab to mitigate undesired interactions due to the periodic images. In sensing applications, the change in the band gap is more significant than its absolute value. So, GGA-PBE functional [37] and DFT-D correction methods proposed by Grimme [38] were selected due to their computational efficiency and consistency with previous DFT studies focusing on gas and bio-sensing [24,39]. The geometry of the BeS monolayer was optimized using the DMol³ module until force and energy met the convergence thresholds of 1.0×10^{-4} Ha per Å and 1.0×10^{-7} Ha between two consecutive steps. The Fermi level smearing parameter of 0.005 Ha was utilized alongside a Monkhorst Pack grid with dimensions of 16×16×1. A global orbital cutoff of 5.0 Å was employed, complemented by the numerical atomic orbital-based Double Numerical Polarized (DNP) basis set. Following this setup, VOCs were introduced to primary adsorption sites to ascertain the most stable and optimal adsorption site. Each volatile organic compound was investigated across four distinct adsorption sites, which encompassed the region between the Be-S bond (designated as the bridge site), the top of the Be atom, the top of the S atom, and the midpoint of the hexagon (referred to as the hollow site). Following the adsorption process, the structures underwent relaxation

utilizing the same parameters employed in the structural relaxation of the pristine monolayer. The adsorption energy of VOC-adsorbed systems and charge transfer between the VOC and the BeS was calculated using the following equations [40] :

$$E_{ad} = E(adsorbate + BeS) - E(BeS) - E(adsorbate) \quad (1)$$

$$\Delta\rho = \rho(adsorbate + BeS) - \rho(BeS) - \rho(adsorbate) \quad (2)$$

Here, E_{ad} is the adsorption energy, $E(adsorbate)$ is the energy of the VOC, $E(adsorbate + BeS)$ is the energy of the VOC-adsorbed BeS monolayer and $E(BeS)$ corresponds to the energy of the BeS monolayer. A more negative value of E_{ad} suggests a robust exothermic interaction and stable adsorption under thermal conditions. In the subsequent analysis, only the configurations with the highest energy favorability were considered.

$\rho(adsorbate + BeS), \rho(BeS), \rho(adsorbate)$ denotes the charge on the VOC-adsorbed BeS monolayer, pure BeS monolayer and the VOC, respectively

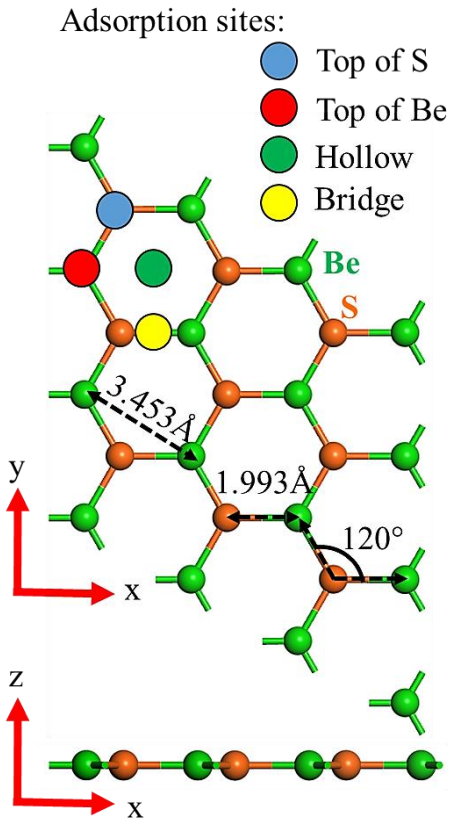


Figure 2. Optimized structure of pristine BeS monolayer's top view and side view. Four adsorption sites on the pristine BeS monolayer are indicated by blue (Top of S), red (Top of Be), green (Center of the hexagon) and red (Between Be-S bond) circles.

Result and discussion

A. Benchmarking Simulation Methodology and Parameters

At first, electronic and structural characteristics of pristine BeS monolayer were computed to establish a benchmark for the simulation methodology. **Figure 2** displays the top views and side views of the pristine monolayer. BeS monolayer exhibits a planar arrangement with a lattice constant of 3.459\AA , a bond length of 1.993\AA and a bond angle of 120° . The band structure and DOS of the pristine monolayer are shown in **Figure 3 (a & b)**. It was found that the BeS monolayer has a band gap of 4.529 eV . These findings align with previous theoretical investigations [34,41,42]. As there is no negative frequencies present in the **Figure 3(c)** the pristine monolayers of BeS can be considered stable.

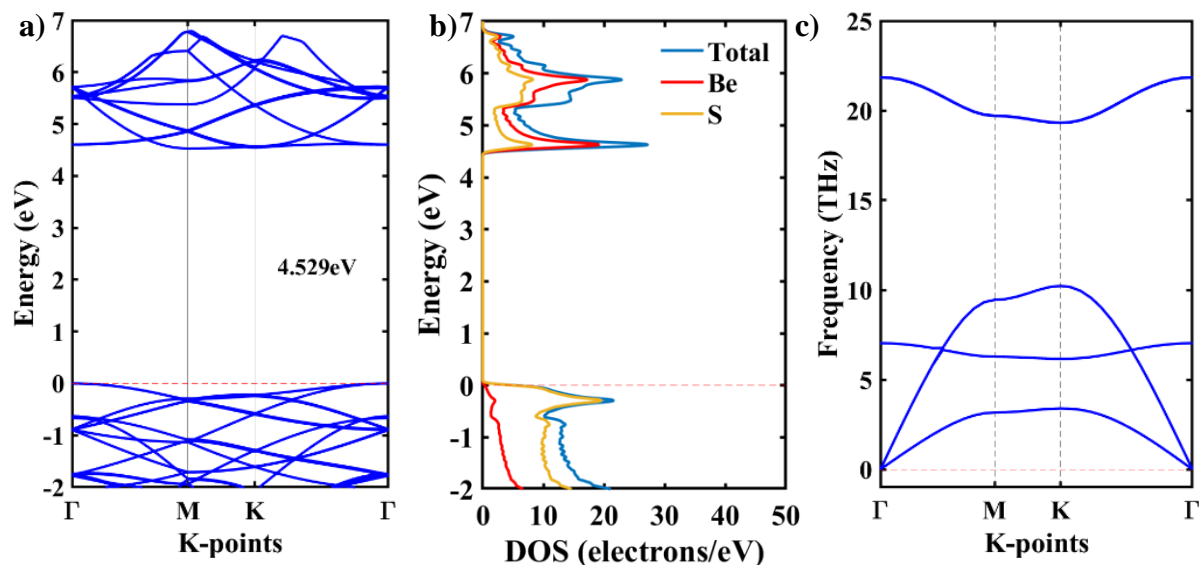


Figure 3. BeS monolayer's (a) band structure (path Γ -M-K- Γ), (c) density of states and (d) phonon dispersion of pristine BeS monolayer

B. VOCs Adsorption on BeS Monolayer

As mentioned earlier, four individual adsorption locations for each VOC, including the center of the hexagon (referred to as the hollow site), the area between the Be-S bond (referred to as the bridge site), the top of the Be atom and the top of the S atom was considered. Only the most stable and energy-favorable adsorption geometries of all BeS analyte systems are demonstrated in **Figure 4**. Different VOCs display affinities for different adsorption sites.

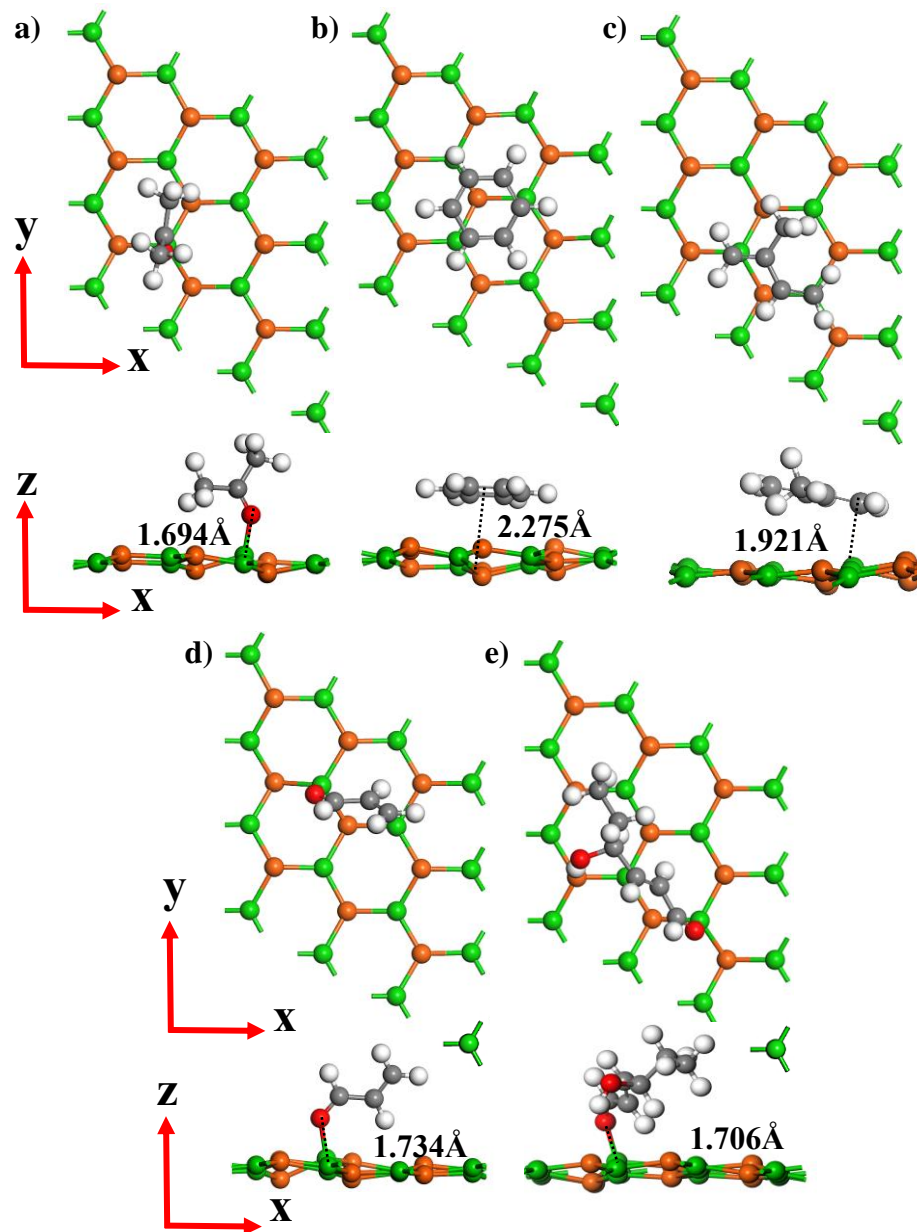


Figure 4. The most optimized structure (top view and side view) for (a) acetone, (b) benzene, (c) isoprene, (d) 2-propenal and (e) 4-hydroxy hexanal (4HHE) on pristine BeS surface. Green, orange, grey, white, and red spheres represent Be, S, C, H, and O atoms, respectively.

Observations of fluctuations in the shortest observed distance (D) between the VOC molecules and the pristine monolayer surface have been noted. The bonding process between the monolayer and VOC molecules is influenced by intermolecular distance, which plays a significant role in defining the adsorption process. In **Table 1**, adsorption energy (E_{ad}), adsorption distance (D), charge transfer (Q), band gap (E_g), band gap change compared to pristine ($\% \Delta E_g$), work function (Φ), recovery time and desorption temperature (T_D) have been summarized for all BeS analyte

systems. If the value of Hirshfeld charge transfer $Q(e)$ is positive (negative), then VOC is considered to be a donor (acceptor). All the charge density difference plots are provided in the supplementary document **Figure S1**. Recovery time and desorption temperature are indicators of the reusability of the biosensor. The adsorption of any VOCs may occur in two ways: physisorption and chemisorption. The E_{ad} is reduced in physisorption, binding the VOC molecule to the substrate through weak vdW (van der Waals) forces, with minimal charge transfer between the substrate monolayer and VOC molecule. Conversely, chemisorption involves a chemical interaction between the VOC molecule and substrate material, characterized by high adsorption energy and substantial charge transfer, leading to a strong charge transfer between the substrate monolayer and VOCs. There is a clear correlation between adsorption energy and material sensitivity. A higher adsorption energy indicates a stronger interaction between the monolayer and VOC molecules, enhancing the material's sensitivity. On the contrary, strong interaction impedes the desorption of VOC molecules from the material's surface, presenting obstacles to the reusability of gas sensors [43,44].

Regarding the adsorption of acetone on BeS, the preferred adsorption site is deemed to be atop the Be atom, as depicted in **Figure 4(a)**. A bond was formed between the O atom of VOC and the Be atom of the pristine monolayer, and the bond length was observed to be 1.694Å. Table 1 shows that the charge transfer between the VOC and pristine is 0.343|e|, and the adsorption energy is -0.845eV. The charge transfer can be visualized from **Figure S1(a)**, where a negative charge was accumulated near the O atom, and the charge was depleted from the surface of pristine BeS. These findings are indications of strong chemisorption. From **Figure 4(b)**, it can be observed that for the adsorption of benzene on BeS, the most stable site was found to be on top of the S atom. The distance between the S atom and C atom was 2.275Å, and the charge transfer was 0.055|e|. Adsorption energy was -0.528eV. Lower adsorption energy, smaller charge transfer, and higher adsorption distance indicate that the interaction was of a physisorption nature. For isoprene in **Figure 4(c)**, the adsorption distance was 1.921Å on top Be atom, charge transfer was 0.258|e|, and adsorption energy was -0.551eV and it was physisorbed. For the adsorption of 2-propenal as shown in **Figure 4(d)**, the adsorption distance was 1.734Å, charge transfer was 0.282|e|, and adsorption energy was -0.763 eV. In this scenarios, a bond was established, and the interaction between the VOCs and pristine BeS was of a chemisorption nature. Highest adsorption energy of -1.141eV was observed in case of adsorption of 4-hydroxy hexanal (4HHE) on BeS monolayer and bond length was observed to be 1.706Å. From **Table 1**, it can be also observed that charge transfer between 4HHE and BeS monolayer is also significant.

Table 1. Adsorption energy (E_{ad}), Hirshfeld charge transfer (Q), adsorption distance (D) observed bandgaps (E_g) for all adsorbed systems and corresponding bandgap change with respect to the pristine BeS, work function (Φ), recovery time of the VOC-BeS system and desorption temperature (T_D)

System	E_{ad} (eV)	Q (e)	D (Å)	E_g (eV)	$\% \Delta E_g$	Φ (eV)	Recovery Time @298K (s)	Recovery Time @298K and UV(s)	T_D (K)
Pristine BeS	-	-	-	4.529	-	6.56	-	-	-
C ₃ H ₆ O - BeS	-0.845	0.343	1.694	2.581	43.01	5.93	19.72	0.019	411.16
C ₆ H ₆ - BeS	-0.528	0.055	2.275	4.292	5.23	6.59	8.58×10^{-5}	8.58×10^{-8}	294.45
C ₅ H ₈ - BeS	-0.551	0.258	1.921	3.534	21.97	6.28	2.08×10^{-4}	2.08×10^{-7}	315.83
C ₃ H ₄ O - BeS	-0.763	0.482	1.734	1.512	66.62	6.01	0.81	8.1×10^{-4}	309.83
C ₆ H ₁₀ O ₆ - BeS	-1.141	0.438	1.706	1.920	57.61	6.23	1.97×10^6	1.97×10^3	334.38

From **Table 2**, it can be observed that charge transfer between the VOCs and pristine BeS was significantly higher for acetone, isoprene, and 2-propenal compared to that of other monolayers for sensing. Charge transfer for benzene was also higher compared to most of the Ti₃C₂MXenes.

C. The stability analysis

Before investigating the electronic and optical properties of different VOC-adsorbed systems, the phonon spectra of these systems were analyzed to ensure the system's stability. As illustrated in **Figure 5**, no negative frequencies were observed in the phonon spectra of any VOC molecules. Also, thermodynamic stability of each VOC adsorbed system can be verified from **Figure S2**.

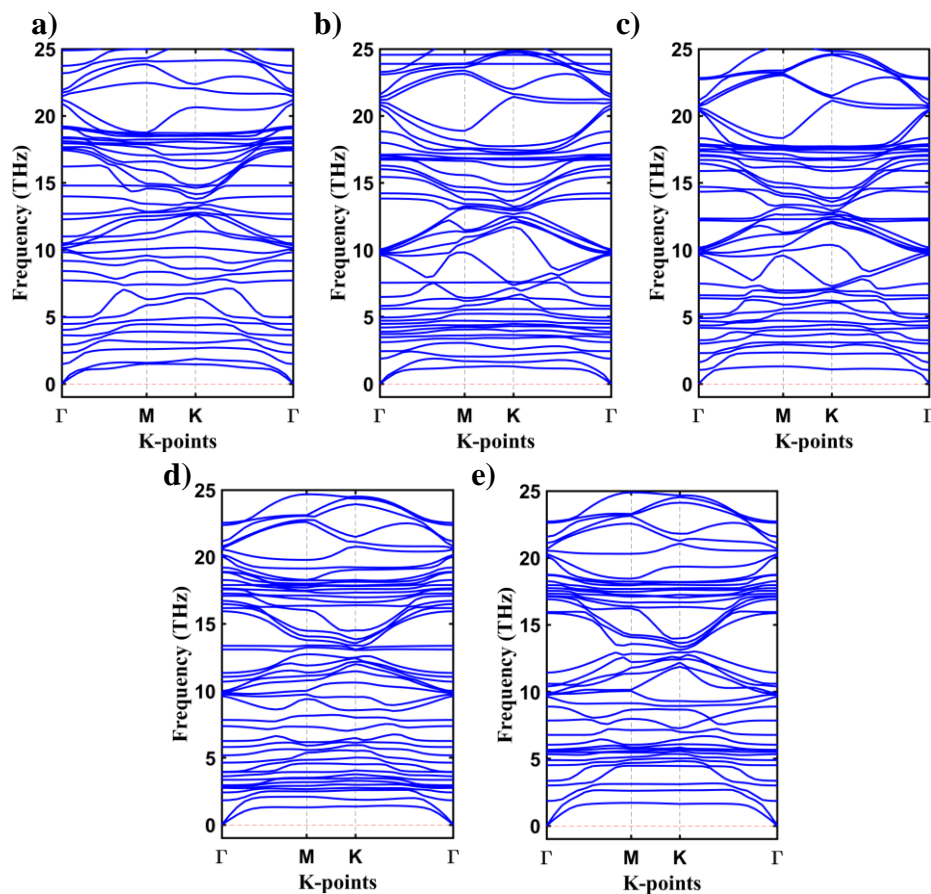


Figure 5. Phonon dispersion of (a) acetone , (b) benzene , (c) isoprene, (d) 2-propenal and (e) 4-hydroxy hexanal (4HHE) adsorbed structure.

D. The Electronic Properties of BeS-analyte System

The analysis involved studying the band structure and partial density of states (PDOS) of both the pristine monolayer and the BeS monolayers adsorbed with various VOCs, as the adsorption of different VOCs induces modifications in the electronic properties of the monolayer. **Figure 6(a)** illustrates the band structure of acetone adsorbed BeS. The bandgap was observed to be 2.581eV. It is significantly reduced compared to the band gap of pristine BeS. The PDOS plot in **Figure 6(a)** helps better understand the role played by the adsorbate molecules in altering the electronic structure of the BeS monolayer. Strong hybridization was contributed by the p orbital of C and O atoms, and the s orbital of the H atom was observed near the 2.5eV region. Hybridization occurs within the forbidden band region of the pristine BeS monolayer, resulting in a substantial 43.01% reduction in the bandgap.

Similar phenomena are also observed when isoprene, 2-propenal and 4HHE is adsorbed on BeS monolayer. From **Figure 6(c-e)**, it can be observed that the change in that bandgap is 21.97%, 66.62% and 57.61% due to the adsorption of isoprene, 2-propenal and 4HHE respectively. It is worth mentioning that the bandgap of the BeS-isoprene system is indirect.

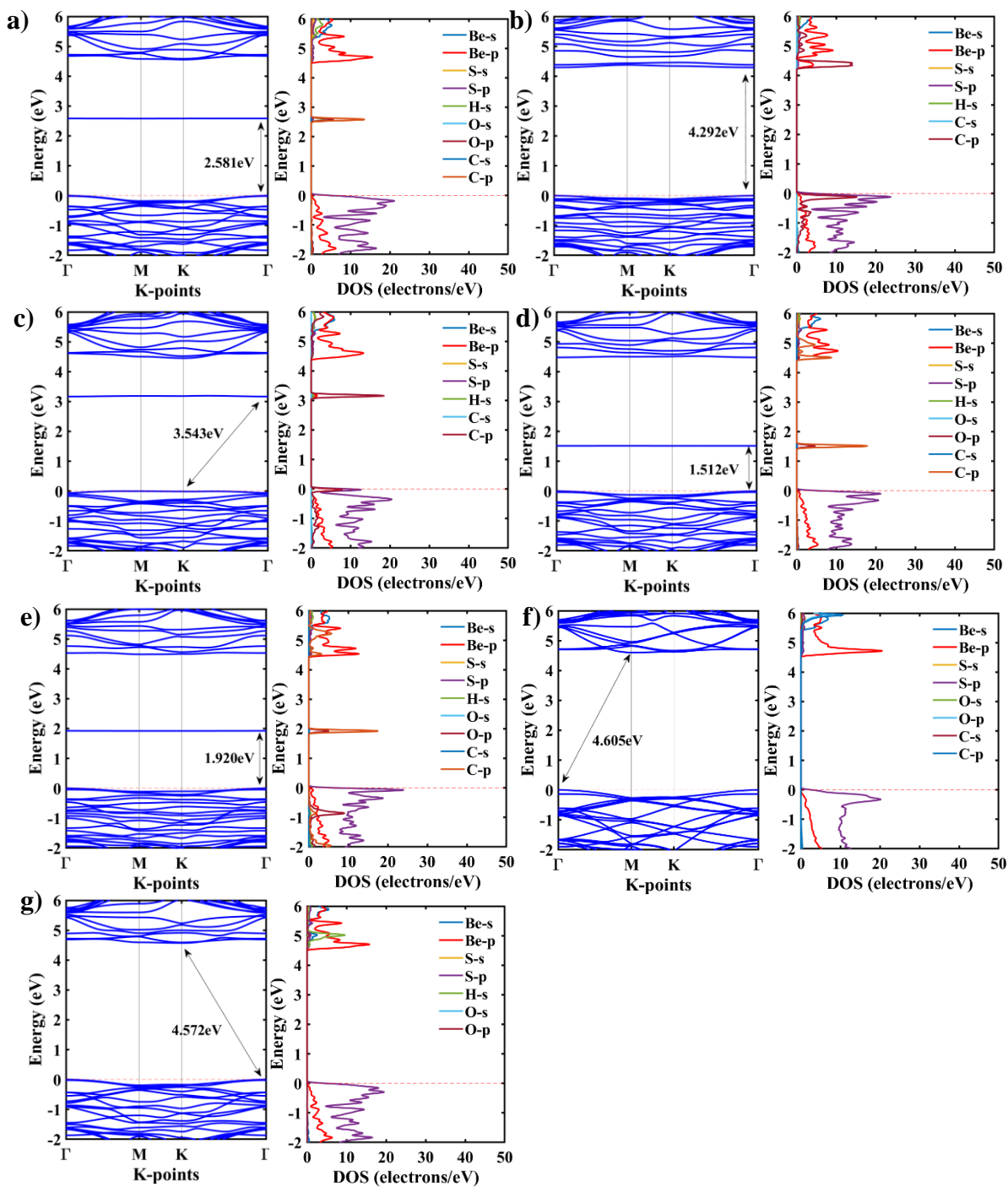


Figure 6. Band structure (path Γ -M-K- Γ) and density of states for (a) acetone, (b) benzene, (c) isoprene, (d) 2-propenal, (e) 4-HHE, (f) CO₂ and (g) H₂O.

By looking at **Figure 6(c-e)**, hybridization between the p orbital of C and O atoms causes defects at 3eV, 1.5eV and 2eV region, respectively. The presence of defect states leads to a reduction in the bandgap of the VOC adsorbed system in comparison to the pristine BeS monolayer.

However, **Figure 6(b)** depicts that when benzene was adsorbed on the pristine BeS, the change in electronic structure was minimal. Analyzing the PDOS plot shown in **Figure 6(b)**, the contribution of the p orbital of the C atom near the conduction band minima and valence band maxima reduced the bandgap by 5.23%.

E. The Optical Properties of BeS-analyte System

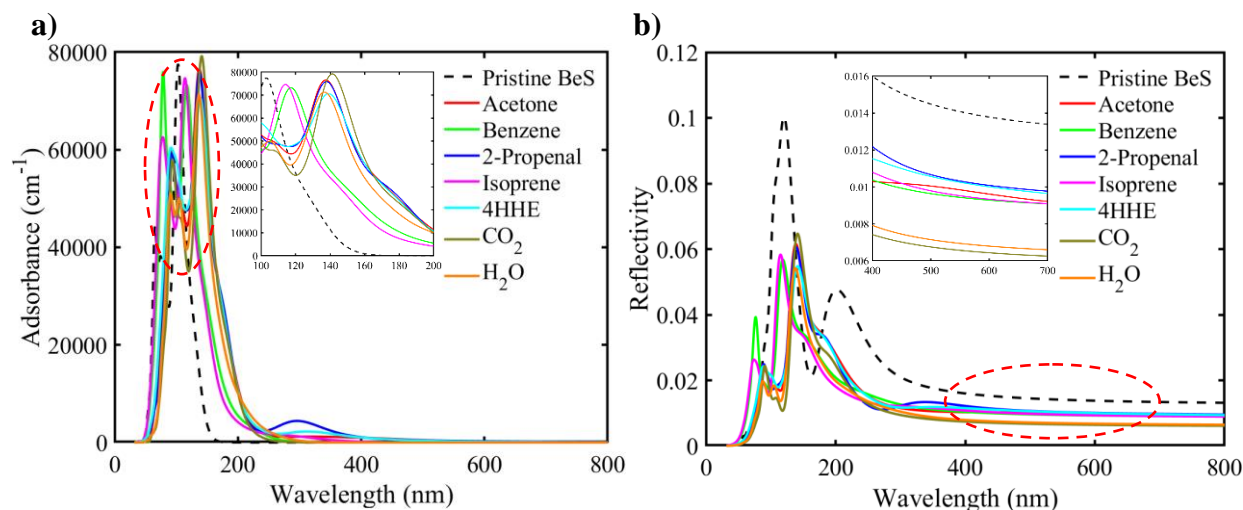


Figure 7. Calculated (a) Absorbance and (b) reflectivity for VOCs and interfering molecules adsorbed on BeS monolayer

In recent years, optical biosensors have gained attention due to their ability to detect changes in a material's optical properties caused by adsorbate molecules [45]. This phenomenon holds promise for selectively sensing volatile organic compounds (VOCs), offering advantages over traditional electrical sensors like immunity to electromagnetic interference and high sensitivity [46]. Additionally, optical biosensors can detect a wide range of molecules by tuning the sensor's frequency. Consequently, exploring whether the BeS monolayer could serve as an effective optical biosensing material with tailored optical properties for different VOCs is crucial. To assess this, absorption coefficient and reflectivity calculations have been performed for various VOC and interfering molecules, such as H₂O and CO₂ adsorbed systems, aiming to determine the BeS monolayer's suitability for selective VOC sensing applications. When light is incident on the VOC-adsorbed BeS structure, major absorption peaks occur between 100~200nm region, as seen in **Figure 7(a)**. The benzene and isoprene adsorbed structures exhibit peak absorbance around 120nm, enabling their selective detection. However, other volatile organic compound (VOC)

molecules, as well as interfering molecules, demonstrate peak absorbance near 140nm, posing challenges for selectivity. Moreover, no light absorption occurs in the visible range.

Reflectivity is a critical optical property for consideration in two-dimensional biosensors due to their reduced thickness. Within the visible region (400nm to 700nm), all volatile organic compounds exhibit over 20% reflectivity, distinguishing them from interfering molecules as shown in **Figure 7(b)**.

E. Work Functions of BeS-Analyte System

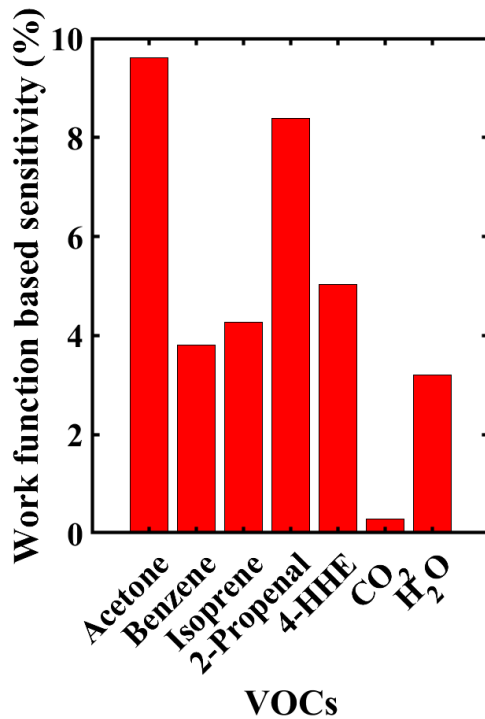


Figure 8. Work function-based sensitivity for different VOC adsorbed system

Work function (Φ) for pristine and different VOC adsorbed structures was determined using the following formula [47]:

$$\Phi = V_{\infty} - E_F \quad (4)$$

Where V_{∞} is the electrostatic potential, and E_F is the fermi potential.

Sensors based on work function can achieve micro gas sensors with minimal power consumption, making them well-suited for cost-effective applications[48]. From **Table 1**, the work function of the pristine BeS monolayer is observed to be 6.56eV. Work function due to the interaction of ambient molecules such as CO₂ and H₂O is 6.585 and 6.340 [34]. **Figure 8** illustrates the work function-based sensitivity, which was calculated using the following equation: -

$$S = \frac{|\Delta\Phi|}{\Phi} \times 100\% \quad (5)$$

The increase in work function was more pronounced for the adsorbed structures of acetone and 2-propenal, measuring 9.603% and 8.38%, respectively. Conversely, the work function shifts induced by the adsorption of benzene, isoprene and 4HHE measured slightly higher at 3.81%, 4.27% and 5.03%, respectively, compared to the shift caused by the adsorption of ambient molecule H₂O. However, the impact of CO₂ is minimal due to its lower sensitivity.

F. Conductivity of BeS-Analyte System

2D nanomaterial demonstrates promise as chemiresistive sensors due to their large surface area, charge transfer mechanisms and compatibility with flexible electronics to revolutionize gas sensing capabilities [49,50]. The Presence of particular VOCs can alter the conductive property of the pristine monolayer. The conductivity of a material is directly related to the bandgap by the following equation [28] :-

$$\sigma = A \exp\left(\frac{E_g}{2k_B T}\right) \quad (6)$$

The following formula can be used to define the change in conductivity:

$$\%S\left(\frac{\delta\sigma}{\sigma}\right) = \frac{\exp\left(\frac{-E_g(\text{adsorbed})}{2k_B T}\right) - \exp\left(\frac{-E_g(\text{pristine})}{2k_B T}\right)}{\exp\left(\frac{-E_g(\text{pristine})}{2k_B T}\right)} \times 100 \quad (7)$$

Here, k_B defines the Boltzmann constant and T is room temperature (298K). $E_g(\text{adsorbed})$ and $E_g(\text{pristine})$ are the bandgap of VOC adsorbed BeS monolayer and pristine BeS monolayer. **Table 1** shows that when 2-propenal is adsorbed, there's a significant 66.62% decrease in the bandgap. Similarly, the adsorption of acetone and 4HHE reduces the bandgap by 43.01% and 57.61%, respectively. These drastic changes in bandgap strongly affect conductivity. 21.97% reduction in bandgap also shows effect in conductivity change due to adsorption of isoprene. Also, it can be observed from **Table 2** that the percentage change in bandgap for these VOCs is significantly higher compared to that of other monolayers. However, when benzene is adsorbed, the bandgap only changes by 5.52%, which is still higher than the changes caused by interfering molecules like H₂O and CO₂, which are only 0.04% and 1.63%, respectively.

G. Recovery time

In sensing applications, recovery time refers to the duration it takes for the sensing materials to revert to its original state after interacting with target molecules. A shorter recovery time can enhance the efficiency and throughput of the biosensing system. Extended recovery time could result in residual molecules from prior measurements interfering with subsequent detections, potentially leading to inaccurate results. The amount of time required for recovery was determined by applying the Van't Hoff-Arrhenius equation.[51]

$$\tau = v_0^{-1} \exp\left(\frac{-E_{ad}}{k_B T}\right) \quad (8)$$

where T is the temperature in kelvin, and v_0 is the attempt frequency. Prior studies established that the attempt frequency of benzene and acetone was 10^{13} Hz [52,53]. Based on previous research, it

is reasonable to presume a similar attempt frequency for other VOCs. **Table 1** presents data regarding the recovery times of various molecules under visible light at a temperature of 298K. Due to physisorption, recovery time for benzene was lesser compared to other VOCs. It has been noted that ultraviolet (UV) radiation aids the sensor's recovery by lowering the desorption barrier [54]. Additionally, **Table 1** demonstrates that under UV light, the recovery time can be decreased at a temperature of 298K. During exposure to UV radiation, the attempt frequency was estimated to be approximately 10^{16} Hz [55]. From **Table 2**, it is evident that the recovery time for some VOCs on SnS₂ is less than nanoseconds. This short time is not suitable for VOC sensing. Conversely, metal-doped MoS₂, SnS₂, and MoSe₂ exhibit significantly longer recovery times for most scenarios, ranging from 3.26×10^{12} to 6.56×10^{31} seconds. In these instances, the material's reusability cannot be guaranteed. However, BeS demonstrates a moderate recovery time, ensuring the sensing material's reusability.

H. Temperature Effect

Below a specific temperature threshold, the adsorption process is spontaneous and energetically favorable, aiding in the loading of VOC molecules onto the nanosheet through physisorption or chemisorption. Since DFT calculations are conducted at 0K, the desorption temperature for each VOC was determined for the real-world environmental assessment using the Van't Hoff equation [56].

$$T_D = \frac{E_{ad}}{k_B} \left[\frac{\Delta S}{R} - \ln \frac{P}{P_0} \right]^{-1} \quad (9)$$

In this equation, E_{ad} represents the adsorption energy, and P stands for pressure, with a reference pressure P_0 set at 1 atm. R represents the universal gas constant and ΔS signifies the entropy change of the VOC. The variation of thermodynamic properties for all the VOCs is shown in **Figure S3**. **Table 1** indicates that at a pressure of 1 atm, the desorption temperatures for acetone, isoprene, 2-propenal and 4HHE are 411.16K, 315.83 K, 309.83K and 334.38K, respectively. Interestingly, the desorption temperatures are above the ambient temperature in these instances. However, for benzene, the desorption temperature is theoretically observed to be lower than room temperature, specifically 294.45 K.

I. Effect of interfering molecules

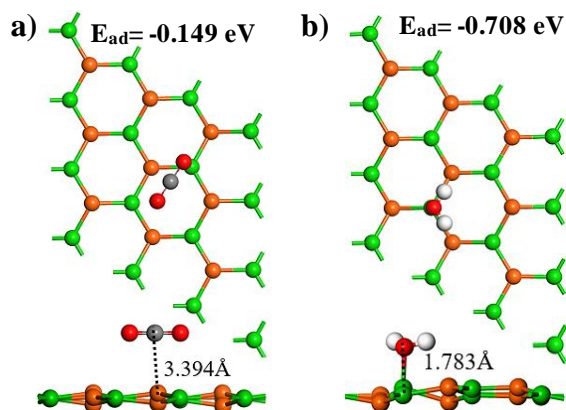


Figure 9. Optimized geometry (top and side view), (a) CO₂ and (b) H₂O adsorbed structure

To ensure selectivity, it's essential to analyze the effects of ambient molecules such as carbon dioxide (CO₂) and humidity (H₂O) on the sensing mechanism. **Figures 9(a)** and **9(b)** depict the geometry of the adsorbed structure in the presence of these molecules. The adsorption of CO₂ has minimal impact on the pristine BeS monolayer, with a lower adsorption energy of -0.149 eV. Moreover, it doesn't alter the electronic band structure significantly, resulting in only a 1.63% change in the band gap. This is validated by the PDOS plot in **Figure 6(e)**, which shows no hybridization near the CBM or VBM and in the forbidden region. The charge transfer is notably low at 0.004|e|, indicating that CO₂ is physisorbed, with its effect being negligible. Similarly, the presence of humidity also slightly affects the electronic structure and PDOS, as depicted in **Figure 6(f)**. Notably, only a 0.04% change in bandgap is observed due to H₂O. However, the adsorption energy and charge transfer for water are higher compared to carbon dioxide, suggesting bond formation. Nevertheless, the adsorption energy of most VOCs remains higher than that of ambient molecules.

J. Enhancing Sensing Response Through Strain

Previous studies have shown that applying strain has the potential to significantly enhance sensitivity by precisely manipulating the atomic scale of graphene nanosheets [57,58]. Due to the graphene-like hexagonal structure of the BeS monolayer, this study investigated its strain-induced sensing response. The percentage of strain can be calculated from the following formula

$$\epsilon = \frac{a - a_0}{a_0} \times 100 \quad (10)$$

where a_0 is the lattice parameter of the BeS monolayer at no strain, and a is the lattice parameter after introducing strain. Both uniaxial and biaxial strains have been applied to test the performance, as depicted in **Figure 10**. The adsorption structures of all VOCs exhibited a consistent trend in response to applied strain. Tensile strain led to a decrease in adsorption energy, prompting the desorption of molecules. Conversely, compressive strain notably enhanced the adsorption energy.

Uniaxial strain applied in both the a and b directions resulted in similar patterns of adsorption energy. For acetone and benzene, the uniaxial compressive strain demonstrated greater enhancement in adsorption energy compared to the biaxial strain. However, for 2-propenal, biaxial compressive strain showed better performance. Intriguingly, all types of compressive strains ranging from -2% to -4% resulted in enhanced adsorption. In conclusion, compressive strain within the range of -2% to -4% is optimal for enhancing the adsorption of VOCs on the BeS monolayer.

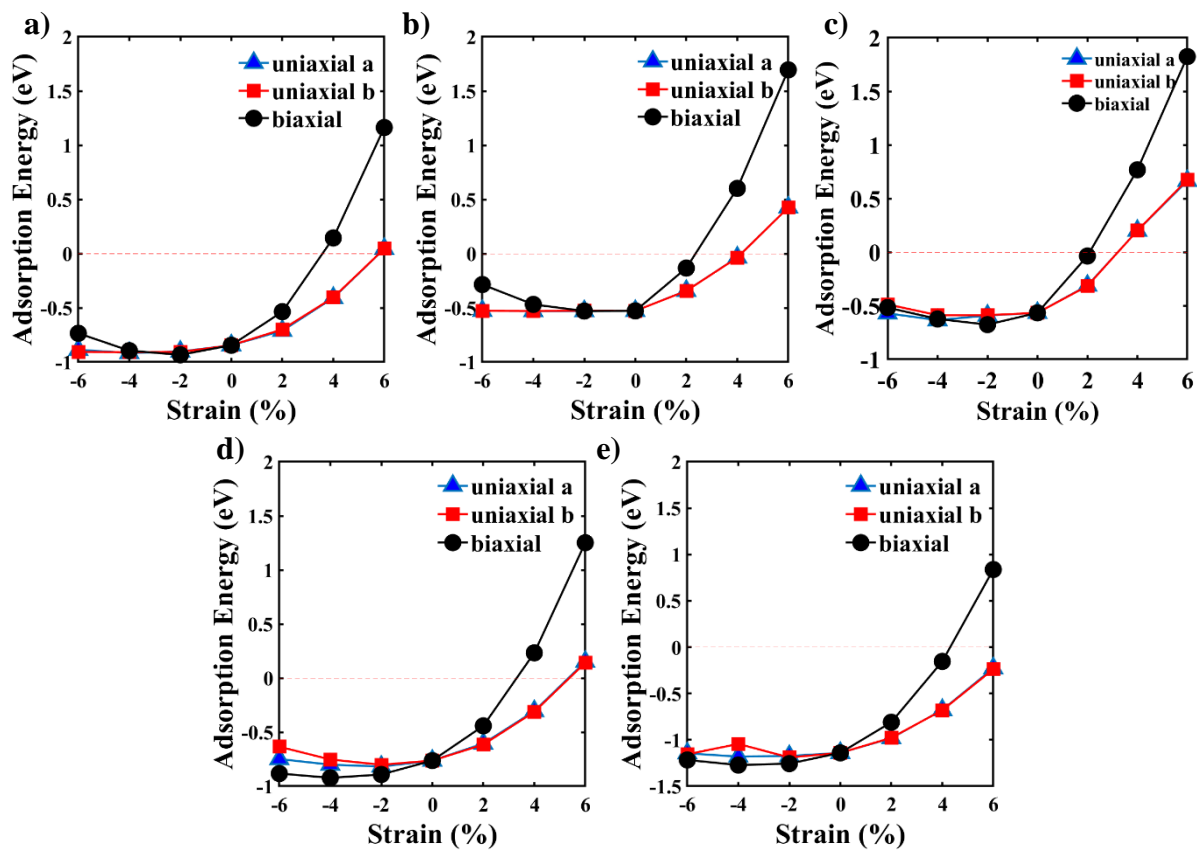


Figure 10. Adsorption energy versus applied strain for (a) acetone, (b) benzene, (c) isoprene, (d) 2-propanal and (e) 4-hydroxy hexanal adsorbed on BeS monolayer

K. Enhancing Sensing Response Through Vertical Electric Field

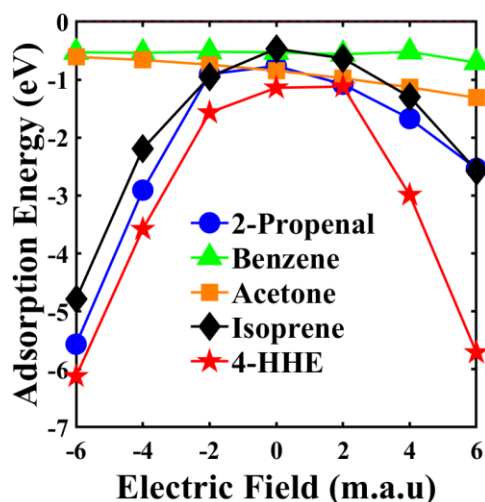


Figure 11. Adsorption energy versus applied electric field for acetone, benzene, isoprene, 2-propenal and 4HHE adsorbed BeS monolayer. The electric field is applied perpendicular to the BeS monolayer, with its positive direction oriented upward along the z-axis. (1 milli atomic unit (m.a.u) = 5.14×10^6 V/cm)

Prior studies showed Applying an electric field vertically significantly improves the sensing performance of the material [59,60]. **Figure 11** illustrates the impact of the vertically applied electric field. For acetone and benzene, a positive electric field strengthens the adsorption energy up to -1.858 eV and -1.028 eV, respectively, while a negative electric field reduces the adsorption temperature. In these cases, the electric field can be utilized to both adsorb and desorb volatile organic compound (VOC) molecules from the surface of the BeS monolayer. Interestingly, for 2-propenal, isoprene and 4HHE, both positive and negative electric fields increase the adsorption energy of the configuration. With a positive 6 m.a.u, the adsorption energy can reach -5.727 eV for 4HHE.

L. Application Description

Lung cancer patients display altered concentrations of various volatile compounds in their breath. The presence or absence of VOCs can indicate the likelihood of lung cancer [61]. The presence of the VOCs like hydro carbons and benzene derivatives, which are possible markers for lung cancer, is promising to detect the disease through breath analysis [62]. Among the VOCs, acetone serves as an initial biomarker for various diseases, including asthma, CKD, CLD, COPD, cystic fibrosis, diabetes, sleep apnea, malaria, and lung cancer. Similarly, isoprene acts as a biomarker for several diseases, including CLD, cystic fibrosis, diabetes, sleep apnea, and lung cancer [63]. Non-small cell lung cancer (NSCLC) and COPD patients, as well as control smokers, exhibited higher levels of isoprene in their exhaled breath [64]. Additionally, the presence of benzene has been observed in the breath of past smokers, indicating that cancer patients with a history of smoking have higher concentrations of benzene in their breath [65]. 2-propenal has strong correlation with lung cancer. Besides, diseases such as pulmonary fibrosis have shown some correlation with this VOC [66].

On the other hand 4HHE was exclusively found in lung cancer patients and was not detected in the air. Therefore, environmental air does not significantly affect the concentrations of this carbonyl VOC in exhaled breath samples [18,67]. Consequently, it can be inferred that these carbonyl compounds originate primarily from alveolar breath and that their concentrations increase might be able to selectively detect lung cancer.

Various types of VOCs may be present simultaneously, making the classification of specific disease via VOCs is quite challenging. Acetone and isoprene can act as the biomarker for most of lung related disease. Among the VOCs, 4HHE demonstrates a strong interaction with the BeS monolayer, exhibiting the highest adsorption energy compared to other VOCs. Consequently, the recovery time for 4HHE is longer than for other VOCs. Therefore, if the monolayer is exposed to UV light for a certain period, it might be possible that only 4HHE will remain on the monolayer, with all the characteristic indicating its presence. Additionally, applying a positive electric field bias may further enhance the interaction, as the energy of 4HHE becomes more favorable with the applied positive bias compared to other VOCs. The entire process is depicted in **Figure 12**. Since 4HHE is exclusively found in lung cancer effected patient's breath, the proposed monolayer may be able to distinguish lung cancer from other lung diseases. However, the BeS monolayer may not be as effective in specifically distinguishing diseases such as chronic liver disease, chronic obstructive pulmonary disease, cystic fibrosis, diabetes, sleep apnea, and malaria, as these conditions share common biomarkers like acetone and isoprene. This overlap makes it challenging for the BeS monolayer to accurately differentiate between them. Nonetheless, the BeS monolayer can serve as an initial screening tool, indicating the potential presence of one of these diseases.

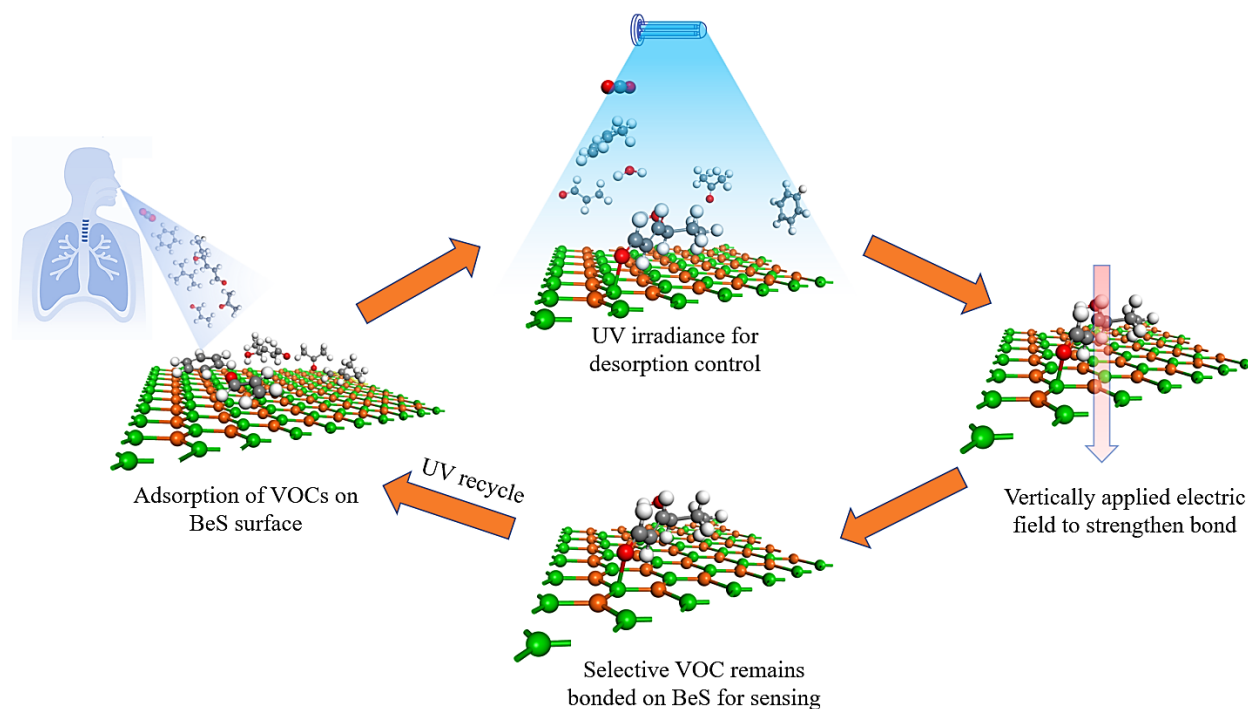


Figure 12. The proposed methodology of BeS monolayer for lung disease diagnosis.

Table 2. Recovery time, percentage of bandgap change with respect to pristine monolayer, and charge transfer for other monolayers.

Monolayer	Recovery time (s) @298K				%ΔE _g				Q (e)			
	C ₃ H ₆ O	C ₆ H ₆	C ₅ H ₈	C ₃ H ₄ O	C ₃ H ₆ O	C ₆ H ₆	C ₅ H ₈	C ₃ H ₄ O	C ₃ H ₆ O	C ₆ H ₆	C ₅ H ₈	C ₃ H ₄ O
BeS	19.72	8.58×10 ⁻⁵	2.08×10 ⁻⁴	0.81	43.01	5.23	21.97	66.62	0.343	0.055	0.258	0.282
MoS₂[24]	-	-	9.16×10 ⁴	27.24	-	-	0.617	1.234	-	-	0.02	0.08
SnS₂[26]	1.31×10 ⁻¹²	3.76×10 ⁻¹³	3.34×10 ⁻¹³	-	-	-	-	-	-	-	-	-
WSe₂[27]	3.94×10 ⁷	-	166.27	-	6.67	-	3.33	-	0.004	-	1.031	-
C-MoS₂[24]	-	-	6.11×10 ²⁵	1.81×10 ²²	-	-	102.8	2.89	-	-	0.032	0.032
Al-MoSe₂[28]	1.82×10 ¹⁸	-	6.47×10 ²¹	3.26×10 ¹²	23.53	-	25	14.7	0.230	-	0.060	0.160
Ni-MoS₂[29]	-	4.70×10 ¹²	1.36×10 ¹⁸	3.79×10 ¹⁶	-	5.58	8.31	7.67	-	0.146	0.191	0.188
Sc-SnS₂[30]	-	7.77×10 ³⁶	6.56×10 ³¹	4.91×10 ¹¹	-	-	-	-	-	0.173	0.249	0.014
Pd-SnS₂[26]	8.02×10 ⁻⁴	2.66×10 ⁻³	16.02	-	25.96	33.6	64.56	-	-	-	-	-
Ti₃C₂O₂[31]	-	8.14×10 ⁻⁴	8.75×10 ⁻³	4.58×10 ⁻⁶	-	-	-	-	-	0.051	0.056	0.017
Ti₃C₂F₂[31]	-	1.47×10 ⁻⁵	2.08×10 ⁻⁴	5.18×10 ⁻⁵	-	-	-	-	-	0.059	0.030	0.032
Ti₃C₂S₂[31]	-	9.28×10 ⁻⁷	2.96×10 ⁻⁴	5.10×10 ⁻⁴	-	-	-	-	-	0.093	0.129	0.102
Ti₃C₂(OH)₂[31]	-	0.11	494.70	2.95×10 ¹⁹	-	-	-	-	-	0.028	0.182	0.372
Ti₃C₂F(OH)₂	-	3.3×10 ⁻³	0.34	8.83×10 ³	-	-	-	-	-	0.203	0.122	0.142

11

Conclusion

In conclusion, this comprehensive study has elucidated the interaction of volatile organic compounds (VOCs) related to various lung diseases with BeS monolayer. Through detailed computational analyses, including electronic band structure analysis, phonon spectra calculations, evaluation of charge transfer, optical property, work function, recovery time assessments, and temperature and interference effects, valuable insights into the feasibility and efficiency of BeS for biosensing applications to detect VOC have been demonstrated. The findings shows significant changes in bandgap upon VOC adsorption, with reductions of 66.62%, 43.01%, and 57.61% observed for 2-propenal, acetone, and 4HHE, respectively. Sensing based on work function was found to be over 5% for acetone, 2-propenal and 4HHE. Regarding optical properties, benzene and isoprene adsorbed structures displayed peak absorbance around 120nm, enabling their selective detection, while within the visible region (400nm to 700nm), all volatile organic compounds exhibited over 20% reflectivity, distinguishing them from interfering molecules. Moreover, recovery times ranging from microseconds to several seconds were evaluated, highlighting BeS's moderate recovery time compared to other 2D materials. Additionally, applying compressive strain in the range of -2 to -4 % and positive vertical electric fields demonstrated promising enhancements in adsorption energy thus improving interaction. The classification of specific VOCs is challenging when multiple VOCs are present simultaneously. Among these, 4HHE exhibits the strongest interaction with the BeS monolayer, having the highest adsorption energy and longest recovery time. Applying a positive electric field bias can further enhance this

interaction, increasing the probability of selective detection. These characteristics underscore BeS's potential as a sensing materials for detection of breath biomarkers responsible for particular lung disease like lung cancer.

Data Availability

The data supporting this article have been included as part of the ESI.

Authors Contribution

Sudipta Saha contributed to the conceptualization, methodology, visualization, software, investigation, drafting of the original manuscript and editing the manuscript. Md. Kawsar Alam was involved in conceptualization, methodology, visualization, resource management, original draft writing, reviewing and editing the manuscript, and provided supervision throughout the research process.

Conflict of Interest

There are no conflicts to declare.

References

- [1] Bray F, Ferlay J, Soerjomataram I, Siegel R L, Torre L A and Jemal A 2018 Global cancer statistics 2018: GLOBOCAN estimates of incidence and mortality worldwide for 36 cancers in 185 countries *CA: A Cancer Journal for Clinicians* **68** 394-424
- [2] Sone S, Takashima S, Li F, Yang Z, Honda T, Maruyama Y, Hasegawa M, Yamanda T, Kubo K and Hanamura K 1998 Mass screening for lung cancer with mobile spiral computed tomography scanner *The Lancet* **351** 1242-5
- [3] Swensen S J, Jett J R, Hartman T E, Midthun D E, Mandrekar S J, Hillman S L, Sykes A-M, Aughenbaugh G L, Bungum A O and Allen K L 2005 CT screening for lung cancer: five-year prospective experience *Radiology* **235** 259-65
- [4] Kim J and Kim K H 2020 Role of chest radiographs in early lung cancer detection *Translational Lung Cancer Research* **9** 522
- [5] Thakur S K, Singh D P and Choudhary J 2020 Lung cancer identification: a review on detection and classification *Cancer Metastasis Reviews* **39** 989-98
- [6] Kikuchi T, Carbone, D. P. 2007 Proteomics analysis in lung cancer: challenges and opportunities *Respirology* **12** 22-8
- [7] Zia K, Siddiqui T, Ali S, Farooq I, Zafar M S and Khurshid Z 2019 Nuclear magnetic resonance spectroscopy for medical and dental applications: a comprehensive review *European Journal of Dentistry* **13** 124-8
- [8] Sodickson A, Baeyens P F, Andriole K P, Prevedello L M, Nawfel R D, Hanson R and Khorasani R 2009 Recurrent CT, cumulative radiation exposure, and associated radiation-induced cancer risks from CT of adults *Radiology* **251** 175-84
- [9] Semelka R C, Armao D M, Elias J and Huda W 2007 Imaging strategies to reduce the risk of radiation in CT studies, including selective substitution with MRI *Journal of Magnetic Resonance Imaging* **25** 900-9

- [10] Altintas Z and Tothill I 2013 Biomarkers and biosensors for the early diagnosis of lung cancer *Sensors Actuators B: Chemical* **188** 988-98
- [11] Ratiu I A, Ligor T, Bocos-Bintintan V, Mayhew C A and Buszewski B 2020 Volatile organic compounds in exhaled breath as fingerprints of lung cancer, asthma and COPD *Journal of Clinical Medicine* **10** 32
- [12] Nooreldeen R and Bach H 2021 Current and future development in lung cancer diagnosis *International Journal of Molecular Sciences* **22** 8661
- [13] Das S and Pal M 2020 Non-invasive monitoring of human health by exhaled breath analysis: A comprehensive review *Journal of The Electrochemical Society* **167** 037562
- [14] Marzorati D, Mainardi L, Sedda G, Gasparri R, Spaggiari L and Cerveri P 2019 A review of exhaled breath: a key role in lung cancer diagnosis *Journal of Breath Research* **13** 034001
- [15] Buszewski B, Ligor T, Jezierski T, Wenda-Piesik A, Walczak M and Rudnicka J 2012 Identification of volatile lung cancer markers by gas chromatography–mass spectrometry: comparison with discrimination by canines *Analytical Bioanalytical Chemistry* **404** 141-6
- [16] Hakim M, Broza Y Y, Barash O, Peled N, Phillips M, Amann A and Haick H 2012 Volatile organic compounds of lung cancer and possible biochemical pathways *Chemical Reviews* **112** 5949-66
- [17] Saalberg Y and Wolff M 2016 VOC breath biomarkers in lung cancer *Clinica Chimica Acta* **459** 5-9
- [18] Fu X A, Li M, Knipp R J, Nantz M H and Bousamra M 2014 Noninvasive Detection of Lung Cancer Using Exhaled Breath *Cancer Medicine* **3** 174-81
- [19] Tao W, Na K, Ji X, Zhang Y, Sharma S, Ouyang J, Qi B, Wang J, Xie N, Kang C and Zhang H 2019 Emerging two-dimensional monoelemental materials (Xenes) for biomedical applications *Chemical Society Reviews* **48** 2891-912
- [20] Bollella P, Fusco G, Tortolini C, Sanzò G, Favero G, Gorton L and Antiochia R 2017 Beyond graphene: Electrochemical sensors and biosensors for biomarkers detection *Biosensors and Bioelectronics* **89** 152-66
- [21] Saha S, Sajib D I and Alam M K 2024 Interaction of the III-As monolayer with SARS-CoV-2 biomarkers: implications for biosensor development *Physical Chemistry Chemical Physics* **26** 6242-55
- [22] Varghese S, Varghese S, Swaminathan S, Singh K and Mittal V 2015 Two-dimensional materials for sensing: graphene and beyond *Electronics* **4** 651-87
- [23] Liu X, Ma T, Pinna N and Zhang J 2017 Two-dimensional nanostructured materials for gas sensing *Two-dimensional nanostructured materials for gas sensing* **27** 1702168
- [24] Karki P, Chettri B, Chettri P, Das S K and Sharma B 2024 Potential application of C-MoS₂ monolayer for identifying lung cancer biomarkers in exhaled breath: a DFT study *Microsystem Technologies* **45** 1-13
- [25] Mosahebfard A and Moaddeli M 2023 MoSe₂ nanosheet as a lung cancer biosensor: A DFT study *Journal of Applied Physics* **134**
- [26] Liu H and Luo X 2023 Au-and Pd-Doped SnS₂ Monolayers for Lung Cancer Biomarkers (C₃H₆O, C₆H₆, and C₅H₈) Detection: A Density Functional Theory Investigation *ACS omega* **9** 7658-67
- [27] Karki P, Chettri B, Chettri P, Das S K and Sharma B 2022 Computation Study of WSe₂ Monolayer for Biomarker in Lung Cancer. In: *2022 IEEE International Conference of Electron Devices Society Kolkata Chapter (EDKCON): IEEE* pp 371-4

- [28] Liu T, Cui Z, Li X, Cui H and Liu Y 2021 Al-doped MoSe₂ monolayer as a promising biosensor for exhaled breath analysis: a DFT study *ACS omega* **6** 988-95
- [29] Zhao G and Li M 2018 Ni-doped MoS₂ biosensor: a promising candidate for early diagnosis of lung cancer by exhaled breathe analysis *Applied Physics A* **124** 1-9
- [30] Verma S, Kumar A, Baghel R and Verma M L 2023 Sc-doped SnS₂ monolayer-based promising biosensor FET for lung cancer early diagnosis: an ab-initio study *Journal of Nanoparticle Research* **25** 130
- [31] Alfalasi W, Hussain T and Tit N 2024 Ab initio investigation of functionalization of titanium carbide Ti₃C₂ MXenes to tune the selective detection of lung cancer biomarkers *Scientific reports* **14** 1403
- [32] Larbi T, El-Kelany K E, Doll K and Amlouk M 2018 Structural stability and vibrational analysis of beryllium sulfide BeS from the bulk to the (n, 0) nanotubes. An ab initio description *Vibrational Spectroscopy* **97** 24-32
- [33] Jalilian J and Safari M 2016 Electronic and optical properties of beryllium sulfide monolayer: Under stress and strain conditions *Physics Letters A* **380** 3546-52
- [34] Zaman A, Shahriar R, Hossain S T, Akhond M R, Mumu H T and Sharif A 2023 A graphene-like BeS monolayer as a promising gas sensor material with strain and electric field induced tunable response: a first-principles study *RSC Advances* **13** 23558-69
- [35] Delley B 2000 From molecules to solids with the DMol 3 approach *The Journal of Chemical Physics* **113** 7756-64
- [36] Clark S J, Segall M D, Pickard C J, Hasnip P J, Probert M I, Refson K and Payne M C 2005 First principles methods using CASTEP *Zeitschrift für Kristallographie-Crystalline Materials* **220** 567-70
- [37] Perdew J P, Burke K and Ernzerhof M 1996 Generalized gradient approximation made simple *Physical Review Letters* **77** 3865
- [38] Grimme S 2006 Semiempirical GGA-type density functional constructed with a long-range dispersion correction *Journal of computational chemistry* **27** 1787-99
- [39] Alfalasi W, Alghoul I, Hussain T, Al-Ali A, Albalooshi A, Aldhanhani M, Al-Sayari H, Ibrahim H and Tit N 2024 Efficient detection of lung cancer biomarkers using functionalized transition metal dichalcogenides (MoS₂) Monolayers: DFT study *FlatChem* **45** 100651
- [40] Nosheen U, Jalil A, Ilyas S Z, Illahi A, Khan S A and Hassan A 2022 First-principles insight into a B₄C₃ monolayer as a promising biosensor for exhaled breath analysis *Journal of Electronic Materials* **51** 6568-78
- [41] Yu J and Guo W 2013 Two-dimensional hexagonal beryllium sulfide crystal *The journal of physical chemistry letters* **4** 1856-60
- [42] Munoz A, Rodríguez-Hernández P and Mujica A 1996 Electronic and Structural Properties of BeSe, BeTe, and BeS: Comparison between ab-initio Theory and Experiments *physica status solidi* **198** 439-46
- [43] Ou P, Song P, Liu X and Song J 2019 Superior sensing properties of black phosphorus as gas sensors: a case study on the volatile organic compounds *Advanced Theory Simulations* **2** 1800103
- [44] Ai W, Kou L, Hu X, Wang Y, Krashennnikov A V, Sun L and Shen X 2019 Enhanced sensitivity of MoSe₂ monolayer for gas adsorption induced by electric field *Journal of Physics: Condensed Matter* **31** 445301

- [45] Bolotsky A, Butler D, Dong C, Gerace K, Glavin N R, Muratore C, Robinson J A and Ebrahimi A 2019 Two-dimensional materials in biosensing and healthcare: from in vitro diagnostics to optogenetics and beyond *ACS nano* **13** 9781-810
- [46] Lei Z L and Guo B 2022 2D material-based optical biosensor: status and prospect *Advanced Science* **9** 2102924
- [47] Gao Q, Zhuang X, Hu S and Hu Z 2020 Corrugation matters: structure models of single layer heptazine-based graphitic carbon nitride from first-principles studies *The Journal of Physical Chemistry C* **124** 4644-51
- [48] Doll T and Eisele I 1998 Gas detection with work function sensors. In: *Chemical Microsensors and Applications*: SPIE) pp 96-105
- [49] Li W-H, Li N, Zhang H, Xu Q and Interfaces 2024 Interfacial Self-Assembly of Oriented Semiconductor Monolayer for Chemiresistive Sensing *ACS Applied Materials*
- [50] Choi S-J and Kim I-D 2018 Recent developments in 2D nanomaterials for chemiresistive-type gas sensors *Electronic Materials Letters* **14** 221-60
- [51] Keleti T a 1983 Errors in the evaluation of Arrhenius and van't Hoff plots *Biochemical Journal* **209** 277-80
- [52] Jyothi M, Nagarajan V and Chandiramouli R 2021 Interaction studies of benzene and phenol on novel 4–8 arsenene nanotubes—A DFT insight *Computational Theoretical Chemistry* **1204** 113381
- [53] Yong Y, Su X, Kuang Y, Li X and Lu Z 2018 B40 and M@ B40 (MLi and Ba) fullerenes as potential molecular sensors for acetone detection: A first-principles study *Journal of Molecular Liquids* **264** 1-8
- [54] Chen R J, Franklin N R, Kong J, Cao J, Tomblor T W, Zhang Y and Dai H 2001 Molecular photodesorption from single-walled carbon nanotubes *Applied Physics Letters* **79** 2258-60
- [55] Aasi A, Aghaei S M and Panchapakesan B 2021 Pt-decorated phosphorene as a propitious room temperature VOC gas sensor for sensitive and selective detection of alcohols *Journal of Materials Chemistry C* **9** 9242-50
- [56] Seenithurai S and Chai J-D 2018 Electronic and hydrogen storage properties of Li-terminated linear boron chains studied by TAO-DFT *Scientific Reports* **8** 13538
- [57] Luo Z, Li X, Li Q, Tian X, Fan T, Wang C, Wu X and Shen G 2020 In Situ Dynamic Manipulation of Graphene Strain Sensor with Drastically Sensing Performance Enhancement *Advanced Electronic Materials* **6** 2000269
- [58] Mehmood A, Mubarak N, Khalid M, Walvekar R, Abdullah E, Siddiqui M T H, Baloch H A, Nizamuddin S and Mazari S 2020 Graphene based nanomaterials for strain sensor application—a review *Journal of Environmental Chemical Engineering* **8** 103743
- [59] Mashhadbani M and Faizabadi E 2023 Enhanced sensing performance of armchair stanene nanoribbons for lung cancer early detection using an electric field *Physical Chemistry Chemical Physics* **25** 29459-74
- [60] Sharma A, Khan M S and Husain M 2019 Adsorption of phosgene on Si-embedded MoS2 sheet and electric field-assisted desorption: insights from DFT calculations *Journal of Materials Science* **54** 11497-508
- [61] Filipiak W, Sponring A, Mikoviny T, Ager C, Schubert J, Miekisch W, Amann A and Troppmair J 2008 Release of volatile organic compounds (VOCs) from the lung cancer cell line CALU-1 in vitro *Cancer Cell international* **8** 1-11

- [62] Di Natale C, Macagnano A, Martinelli E, Paolesse R, D'Arcangelo G, Roscioni C, Finazzi-Agro A and D'Amico A 2003 Lung cancer identification by the analysis of breath by means of an array of non-selective gas sensors *Biosensors Bioelectronics* **18** 1209-18
- [63] Moura P C, Raposo M and Vassilenko V 2023 Breath biomarkers in Non-Carcinogenic diseases *Clinica Chimica Acta* **552** 117692
- [64] Horvath I, Lazar Z, Gyulai N, Kollai M and Losonczy G 2009 Exhaled biomarkers in lung cancer *European Respiratory Journal* **34** 261-75
- [65] Phillips M, Gleeson K, Hughes J M B, Greenberg J, Cataneo R N, Baker L and McVay W P 1999 Volatile organic compounds in breath as markers of lung cancer: a cross-sectional study *The Lancet* **353** 1930-3
- [66] Wu X, Li Z, Shu J, Lu Z, Gao J, Yang B, Jiang K, Guo Y and Huang J 2022 Exploring breath biomarkers in BLM-induced pulmonary fibrosis mice with associative ionization time-of-flight mass spectrometry *Talanta* **239** 123120
- [67] Schumer E M, Trivedi J R, Van Berkel V, Black M C, Li M, Fu X-A and Bousamra II M 2015 High sensitivity for lung cancer detection using analysis of exhaled carbonyl compounds *The Journal of Thoracic Cardiovascular Surgery* **150** 1517-24